Chapter 7

Magnetic Fields in Nearby Molecular Clouds

In Chap. 6, we saw the power of imaging polarimetric techniques in probing the two-dimensional magnetic field patterns associated with Bok globules. Here, we further illustrate the usefulness of imaging polarimetry in studying Galactic extended objects. Observations on two other types of molecular clouds in the Galaxy, namely Cometary globules and filamentary clouds are presented in the following sections.

7.1 Cometary Globules

Globules play an important role in low mass star formation in the interstellar medium (ISM). It was Bart Bok who made the first suggestion that the isolated dark clouds may be potential sites of current star formation. With the advent of infrared and millimeter astronomy, direct observations could be made of the structure and kinematics of these clouds as well as the objects seen in there vicinity (Clemens & Barvainis 1988; Bourke et al 1995a). These studies have found conclusive evidence for the correctness of Bok's prediction (Wang et al 1995; Bourke et al 1995b). More recently, observations of another type of objects called the cometary globules, also indicate signs of recent star formation which is taking place in them (Sugitani et al 1991, SFO hereafter; Sugitani & Ogura K 1995). Several of the as yet poorly understood phenomena associated with star formation are attributed to the interaction between gravity, angular momentum and magnetic field (Wardle & Königl, 1993; Ostriker & Shu 1995).

Morphologically, globules in the ISM can be classified into four types. These are the elephant trunk globules (Schneps et al 1980), teardrop globules (Herbig 1974), both seen profusely in the Rosette nebula, cometary globules (Hawarden & Brand 1976; Sandqvist Aa 1976) seen in large numbers in the Gum nebula and the isolated dark globules, known as Bok globules (Barnard 1919). Compelling evidence accumulated over the last four decades through observations and theoretical modeling has led to the widespread belief that these different types of globules, in fact form an evolutionary

sequence, with the teardrops and Bok globules being the later evolutionary stages of the elephant trunks and cometary globules (eg : Reipurth 1983). On the other hand, the elephant trunks and cometary globules themselves are supposed to be the results of a supernova-induced shock wave or a recent star formation-generated ionization front hitting the nearby cloud (Brand 1983; Reipurth 1983; Schneps et al 1980). Whatever be the underlying mechanism, it is widely believed that the magnetic fields in the region will have an important role to play in the formation and evolution of these globules (eg: Bertoldi & McKee 1990; Lefloch & Lazareff 1994).

As Sridharan et. al. (1996) has pointed out, our understanding of magnetic fields still leaves a lot to be desired, in spite of their recognized importance in investigating the dynamics of the ISM. This can be mainly attributed to the lack of effective observational techniques which can measure the strength of these fields and their three dimensional structure. However, magnetic fields do leave observable imprints on the aspherical, spinning, dichroic dust grains which are present in the ISM, by aligning their axes along the field lines. Thus inference about the orientation of the magnetic field lines projected against the sky may be obtained through polarimetry of starlight scattered through the dust grains.

In their recent study of the cometary globule CG 22 in the Gum nebula, Sridharan et. al. (1996) addresses several questions relating to the effects on and of magnetic fields during the formation and evolution of these globules. The present investigation on two more cometary globules is a follow up to their study. These globules, named S 273 and S 277, were selected from a catalogue of cometary globules in the northern hemisphere, compiled by SFO.

7.1.1 Observations and Results

The observations were made with the 1.2 m GIRT telescope in February 1997. The data of S 273 consist of 12 exposures, three at each of the four half-wave plate positions. The data of S 277 consist of 20 exposures, five at each half-wave plate position. The filter used was the same as that is described in Sec. 6.2.1 – 4 mm thick, Schott KG3 glass, having a bandwidth of about 2000 Å. The details of the procedure employed for acquiring the images and the techniques of data analysis used for extracting polarimetric information from the raw images, are similar to that has been described in Sec. 6.2.1.

S273 appears towards northern Monoceros, in the diffuse HII region associated with the young cluster NGC 2264 (Monoceros OB 1). It has a beautiful boomerang appearance on POSS prints and near its head, the rim shows up as a region of bright emission (see Fig. 7.1(top)). The distance to Monoceros OB 1 has been estimated to be about 780 pc (Turner 1976). S277 is an HII region about 3° north of the Great Orion Nebula. Unlike S273, the tail of this globule converge together behind a dark core in the shadow of the head, to form one diffuse region (see Fig. 7.1(bottom)). Again, the rim near the head appears as a bright nebulous region. This globule is assumed to be at the same distance as Orion nebula, that is about 400 pc away (Bok et al 1971).

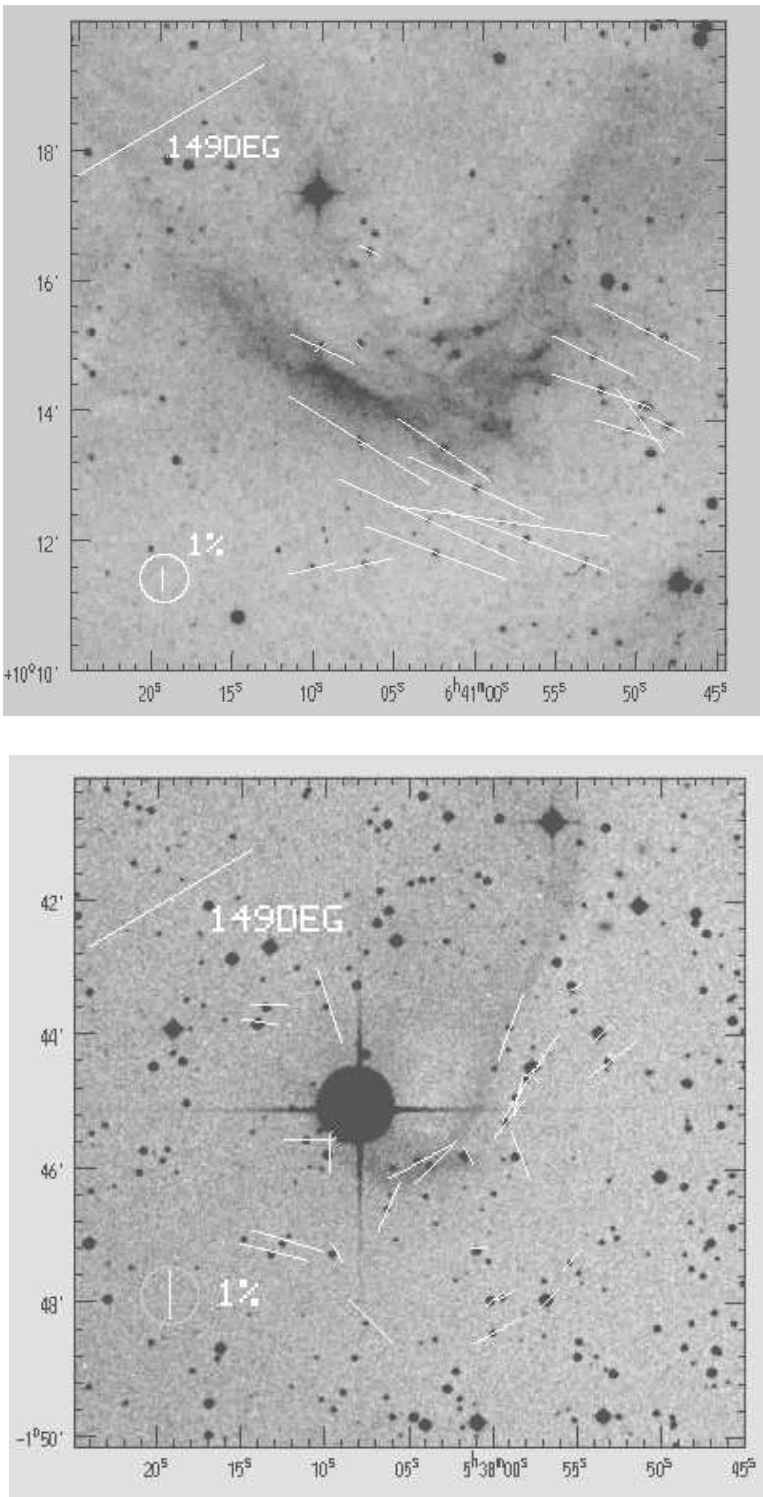

Figure 7.1: (Top) Polarization vector map of the field stars shining through the dust near the cometary globule S273. (Bottom) Polarization vector map of the field stars shining through the dust near the cometary globule S277. The long vectors marked at the NE corner show the approximate direction of the Galactic plane in the region (149°).

Table 7.1: Linear polarization data of stars behind the clouds S273 and S277

(a) S273

No.	p (%)	σ_p (%)	θ (°)	σ_θ (°)	V mag
1	2.34	0.48	166.9	5.9	17.45
2	6.21	0.42	20.5	1.9	15.87
3	7.40	1.20	20.8	4.6	16.76
4	8.98	2.33	8.1	7.4	17.80
5	8.21	1.02	25.0	3.6	16.98
6	6.15	0.21	24.8	1.0	14.96
7	4.63	0.61	34.3	3.8	16.59
8	2.84	0.78	16.8	7.9	17.25
9	6.83	0.34	31.9	1.4	16.01
10	1.64	0.43	27.2	7.4	15.54
11	3.24	1.21	54.0	10.7	17.11
12	0.36	0.12	136.6	10.0	14.09
13	4.32	0.24	19.5	1.6	14.85
14	3.79	0.69	26.9	5.2	16.99
15	4.92	0.72	28.1	4.2	16.58
16	2.86	0.87	24.8	8.7	16.99

(b) S277

No.	p (%)	σ_p (%)	θ (°)	σ_θ (°)	V mag
1	1.05	0.52	152.5	14.1	16.51
2	0.51	0.03	134.4	1.8	12.69
3	0.46	0.14	140.4	9.0	15.06
4	1.47	0.47	15.5	9.2	16.50
5	1.53	0.69	15.4	13.0	16.60
6	1.11	0.24	111.4	6.1	15.66
7	1.00	0.11	67.3	3.2	14.50
8	1.58	0.46	150.3	8.3	16.21
9	0.37	0.09	61.5	6.8	14.08
10	0.80	0.12	91.7	4.2	15.17
11	1.10	0.22	178.7	5.8	15.84
12	0.93	0.30	127.3	9.1	15.79
13	2.14	0.81	122.6	10.8	16.77
14	0.45	0.03	137.2	2.1	12.84
15	1.22	0.26	142.4	6.1	16.09
16	0.41	0.05	132.1	3.2	13.28
17	1.52	0.20	109.6	3.7	15.95
18	0.78	0.05	6.5	2.0	13.18
19	1.62	0.69	70.3	12.1	16.74
20	0.79	0.21	4.3	7.6	15.34

Superimposed on the Digitized Sky Survey grey scale maps of the cloud regions (Fig. 7.1(top) and (bottom)) are vectors showing the degree of linear polarization and position angle for many of the stars. The approximate orientation of the Galactic plane (149°) is shown at the north-east corner of each map. Table 7.1(a) and (b) give the data corresponding to the vectors marked on the maps. p, θ, σ_p and σ_θ are the degree of linear polarization, position angle of polarization and the corresponding 1σ errors, estimated by fitting a cosine curve to the normalized Stokes parameters. V is the visual magnitude of the star.

7.1.2 Discussion

CGs are typically 0.05 to 1 pc in size and have densities between 10^4–10^5 cm^{-3} (Bertoldi 1989). A widely accepted belief is that the cometary globules (CG hereafter) are formed when UV radiation from one or more OB stars disperse the parental molecular cloud, but for a relatively dense clump. The face of the clump where the ionizing front hits it, becomes the bright rim, marking the boundary between the HII region and the surviving part of the molecular cloud. The tails are formed by the material swept away by the radiation. Focusing of the gas by the sweeping radiation leads to implosion of the clump material and consequently star-formation. It has been estimated (SFO) that radiation-driven implosions might be contributing about 5% of the total stellar mass in the Galaxy.

In addition to the inferences from the extensive theoretical modeling (see SFO for a list of references), three direct observational evidences are found in support of the above radiation-driven model for the formation of the CGs. First and foremost is the fact that they are found in/around HII regions. Secondly, they have their tails mostly pointing radially away from a central source. This is particularly noticeable in the case of the large population of cometary globules in the Gum-Vela region, which forms an arc around a central region of massive stars (Sridharan 1992). The two CGs included in this study also have candidate central sources from which the tails appear to point away. And thirdly, the CGs are often found with systematic velocities which indicate that they are accelerating away from the centre of ionizing radiation, with velocities as high as 10 kms^{-1}. This is explained in terms of the 'rocket effect' caused by the anisotropic ejection of ionized gas from the bright rims (Sridharan 1992).

A question which is pertinent to the above scenario of CG formation is whether the clumps will survive the harsh environments, long enough to form stable structures. Given the typical the typical conditions under which CGs are seen, they will outlive the onslaught of the ionizing radiation, provided the material interacts with the magnetic field. (Bertoldi & McKee 1990). For a magnetic cloud the evaporation time will be hundred times more than the time needed to settle into equilibrium configuration. Possible mechanisms by which the cloud material couple to the magnetic field are charged dust grains and photoionization.

CGs show a wide variety of structures – tails which are filamentary and those which are very diffuse; tails which bend sharply and those which curve smoothly. Based on

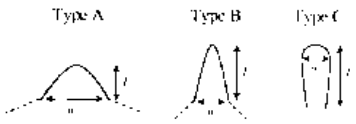

Figure 7.2: Three morphological types of cometary globules. The definitions of the length (l) and width (w) parameters are illustrated for the three types. (adapted from Sugitani et. al. 1991).

the head-tail morphology, SFO have classified CGs into three types as illustrated in Fig. 7.2 (adapted from SFO). Type A have length to width ratio, $\frac{l}{w}$, less than 0.5, type B greater than 0.5 and type C greater than 1. This classification also seems to order the clouds according to the frequency with which they are seen; A being most frequent and C the least. S273 is a B type globule ($l \sim 0.65$ pc, $w \sim 1.22$ pc), while S277 is C type ($l \sim 0.7$ pc, $w \sim 0.2$ pc).

An interesting feature of S273 is that its tail actually has two bright rims on its eastern side. Apparently, the one which has been noted by SFO for their classification is the inner one, which points at about 20° east of north. However, there is another, brighter tail, pointing at about 45° east of north. All the three rims meet at the same head. A possible explanation for reconciling this double-rim structure with the above described scenario for CG formation, is that these two rims are formed as a result of two different instances of radiation dispersal and that the tail is actually formed from material being swept from the head.

The rim on the western side of S273, is quite diffused and has a wind-blown appearance. In S277, the western rim is quite prominent and appears as a clear boundary between the tail and the surrounding medium. However, the eastern side of the tail does not have such clear edge, but is diffuse and gradually merges with the surrounding medium. In fact, a visual inspection of the 44 CGs listed by SFO, shows clearly that assymetric rims and wind-blown appearances are quite common in CGs. These features are particularly noticeable in the case of clouds numbered 1, 2, 12, 14, 16, 17, 19, 20, 22, 25, 28, 34, 37, 39 and 41, in Table 2 of SFO. It is difficult to reconcile the appearance of both sharp rims and wind-blown like boundaries in the same cloud, within the framework of their radiation-driven origin.

Sridharan et al (1996) did polarimetry of a few relatively bright background stars shining through the globule CG 22 whereby they concluded that the magnetic field is quite tightly aligned to the tail of the globule. They speculated that the processes that formed the CGs were also responsible for creating the aligned magnetic field, by stretching the pre-existing field along the tail. If this were true, such aligned magnetic fields should be a general feature of CGs. In the case of the two globules studied in our observation, we find that the stars which are close by to the bright rims have their polarization vectors aligned along the rims – in S273, the stars at the head and the south-east corner of the head and in S277, the stars at the head and the clearly demarked western edge of the CG's tail. If the polarization is due to aspherical dust grains aligned by the magnetic field (Davis & Greenstein 1951), these vectors trace

the direction of the magnetic field, which then does appear to be coupled to the rim structure of the CGs. The fact that the magnetic field alignment is seen along the bright rims of the tails and not along their wind-blown edges, probably indicates that it is the enhancement of free charges at these rims (through dust-charging or photoionization of gas), where the ionization front collides with the clump, which couples the magnetic field to the cloud material. In S277, the magnetic field at the western corner of the head of the CG appears to bend around to follow the western edge of the tail. Such bending of the fields have been observed in the case of L810 and B335 (Hodapp 1987).

7.2 Filamentary Clouds

Filamentary structures are very common in the interstellar medium of our Galaxy. Supernova remnants and many of the dark molecular clouds in the Galaxy display elongated structures. It is not easy to distinguish whether an elongated structure is truly filamentary – that is with very large length to radius ratio – or they are flattened slabs, seen edge on. A difficulty with the filamentary models lies in explaining how they acquire these structures before the gravitational forces were strong enough to contract them. One of the possible mechanisms is based on the large scale currents that permeate the Galactic plasma (Carlqvist 1978; Alfvén 1978). The toroidal magnetic fields associated with these currents provide a pinching force which result in filamentary structures (Alfvén & Carlqvist 1978). Such pinching forces associated with a current sheet can result in flattened slabs too. However, a more attractive mechanism of forming flattened slabs is through gravitational collapse of a cloud which is supported by a largely uniform magnetic field. In such a situation, the collapse occurs mainly along the magnetic flux lines, while in the plane perpendicular to the field, the magnetic pressure support offers resistance to collapse. Such a cloud will be elongated perpendicular to the magnetic field.

Polarimetry of starlight scattered by aligned, dichroic dust grains in the molecular clouds offer a tool for discerning the magnetic field patterns which exist in these clouds. Previous optical and near-infrared polarimetric studies of several elongated molecular clouds have revealed a variety of magnetic field patterns (Myers & Goodman 1981). In many of the clouds, the polarization vectors are predominantly perpendicular to the long axis of the clouds (eg. McGregor et al 1994; Heyer et al 1987). If these vectors trace the orientation of the magnetic fields, these observations go along very well with the flattened sheet models based on gravitational collapse of magnetized clouds. On the other hand, there are several observations in which the magnetic field is claimed to be mostly aligned along the long axis of the cloud (eg. Goodman et al 1990; Vrba et al 1981). To explain these observations, In this context, it is to be noted that the statements about parallel and perpendicular fields, which are made in the above examples are only approximate. The actual position angles show dispersions as large as 30° from the mean values. The truly filamentary clouds, having helical magnetic fields produced by currents, are expected to show a bimodal distribution of polarization position angles centred at 0° and 90°.

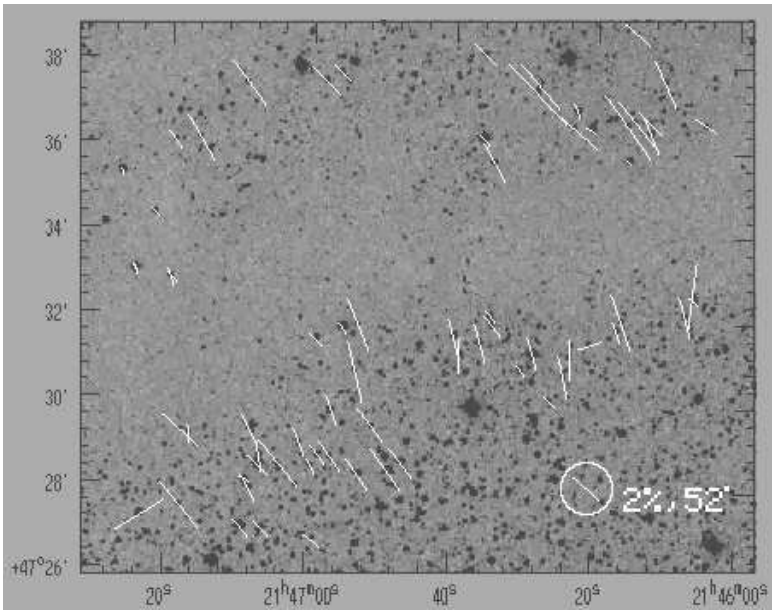

Figure 7.3: Polarization vector map of the field stars shining through the dust in the elongated cloud near IC 5146.

Here, we report the results from polarimetric observations of an elongated cloud complex near the young open cluster IC 5146. This cluster is situated in the direction of Cygnus and has an H II region associated with it. The cloud complex extends more than 2° to the west of the cluster and its overall morphology, as it appears on Palomar Sky Survey blue print, resembles very much, the famous ρ Ophiuchi cloud complex.

7.2.1 Observation and Results

These observations were made with the 1.2 m GIRT on Mt. Abu, during November 1996. The molecular cloud on the west of the cluster actually appears as two large elongated structures, one which is about 1° west of the cluster, and is called southern streamer and another larger one is about 0.3° north of the southern streamer, and is called the northern streamer (Lada et al 1994). In this observation, we have done polarimetry of the eastern part of the northern streamer, which was covered in four, slightly overlapping fields. For each field, four exposures were taken at each of the half-wave plate orientations. Other details of observation and data-analysis remains essentially the same as described in Sec. 6.2.1.

Results of these observations are presented in Fig. 7.3, in which the polarization vectors are superimposed on a Palomar Observatory Sky Survey print of the region. The vector inside the circle is roughly oriented along the direction of the Galactic plane towards IC 5146. The polarimetric data corresponding to the figure is given in Table 7.2.

Table 7.2: Linear polarization data of stars behind the Northern Streamer near IC 5146

No.	p (%)	σ_p (%)	θ (°)	σ_θ (°)	V mag	No.	p (%)	σ_p (%)	θ (°)	σ_θ (°)	V mag
1	1.64	0.10	40.8	1.7	14.28	34	3.18	0.28	45.8	2.5	15.83
2	1.82	0.04	39.4	0.6	12.80	35	4.57	0.63	37.3	4.0	16.13
3	4.63	0.53	122.5	3.3	14.93	36	1.96	0.54	44.9	8.0	16.36
4	1.58	0.64	50.5	11.6	15.84	37	1.11	0.41	45.4	10.6	16.14
5	2.45	0.29	28.4	3.4	15.32	38	3.42	0.50	11.3	4.2	16.21
6	0.77	0.12	49.2	4.6	13.64	39	1.14	0.22	37.8	5.5	14.87
7	3.19	0.16	33.1	1.4	14.63	40	3.19	0.47	1.3	4.2	15.81
8	4.25	0.56	33.7	3.8	17.08	41	2.77	0.11	16.1	1.1	11.48
9	2.98	0.47	38.4	4.5	16.76	42	2.92	0.32	179.4	3.1	14.71
10	1.39	0.18	26.2	3.7	15.25	43	1.98	0.30	108.8	4.3	16.24
11	4.84	0.91	38.8	5.4	16.51	44	3.27	0.16	15.4	1.4	13.73
12	2.22	0.01	46.2	0.2	11.92	45	2.95	0.23	13.7	2.2	13.92
13	3.08	0.30	35.1	2.8	15.31	46	1.79	0.34	20.1	5.4	14.80
14	1.98	0.36	35.0	5.1	15.44	47	2.11	0.13	37.9	1.8	13.75
15	2.55	0.66	9.8	7.3	16.91	48	4.89	0.58	18.0	3.4	15.42
16	2.48	1.27	19.7	14.6	16.62	49	1.26	0.11	37.5	2.5	13.46
17	1.43	0.37	4.7	7.4	16.36	50	3.32	0.18	16.4	1.5	14.33
18	3.93	1.35	47.5	9.9	16.48	51	5.36	0.71	172.4	3.8	16.53
19	2.55	0.23	26.5	2.6	14.75	52	0.48	0.17	42.3	10.1	13.52
20	3.38	0.64	36.9	5.4	16.00	53	3.68	0.10	28.2	0.8	14.18
21	2.54	0.09	22.3	1.0	14.24	54	1.13	0.04	46.1	1.1	12.10
22	5.13	0.85	12.1	4.8	17.11	55	3.28	0.12	20.8	1.1	13.74
23	1.38	0.21	51.1	4.3	14.75	56	0.83	0.10	58.3	3.4	13.01
24	0.95	0.04	38.7	1.1	12.31	57	5.14	0.39	49.6	2.2	15.41
25	4.56	0.45	22.5	2.8	15.88	58	1.99	0.38	54.9	5.5	16.35
26	1.00	0.25	40.8	7.1	14.81	59	6.52	0.71	34.8	3.1	16.61
27	0.79	0.04	31.1	1.3	12.63	60	4.61	0.69	37.2	4.3	16.26
28	1.39	0.16	13.4	3.4	14.93	61	1.28	0.12	19.3	2.6	13.59
29	0.89	0.05	23.7	1.7	12.81	62	6.89	0.24	42.7	1.0	14.83
30	0.72	0.23	40.7	9.3	14.95	63	4.81	0.62	39.9	3.7	16.40
31	0.45	0.06	35.1	3.6	12.93	64	4.21	0.39	22.6	2.7	15.73
32	1.68	0.29	34.8	4.9	14.91	65	2.45	0.27	44.8	3.2	14.43
33	4.28	0.52	30.5	3.5	15.83	66	2.54	0.42	50.3	4.8	15.51

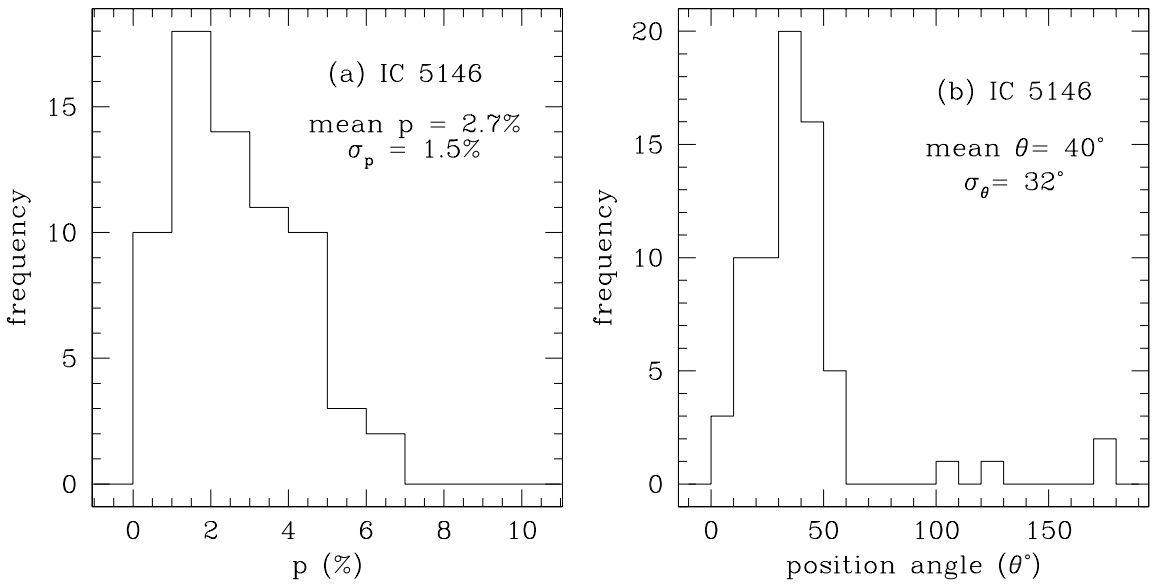

Figure 7.4: (a) Histogram of degree of linear polarization (p). (b) Histogram of polarization position angles (θ). σ_p and σ_θ are the rms dispersion from mean values of p and θ.

7.2.2 Discussion

Fig. 7.4(a) and (b) show histograms of the degree of linear polarization (p) and position angle of the polarization vectors (θ). Both show characteristic peaked structures typical of interstellar clouds. The mean value of polarization is 2.7%, but there is a large scatter of about 1.5% around this mean. The mean position angle is about 40° with an rms dispersion of 32° when all the stars in Table 7.2 are considered. However, it is clear from the histogram there are four stars which show markedly deviant polarization position angles (Star no. 3, 42, 43, 51 in Table 7.2). If these stars are eliminated, the mean value position angle becomes 33° and the dispersion about this mean becomes 13° which is typical of interstellar clouds.

The mean position angle of the polarization vectors is less than 20° away from the direction of the Galactic plane. This indicates that the magnetic field at the periphery of Northern Streamer is moderately coupled to that in the ambient interstellar medium. Besides, the mean polarization is comparable to what one would expect for interstellar scattering over a distance of 1 kpc (see Eq. 6.7), which is the estimated distance to the cluster (Dobashi et al 1992). Thus, in this case, it is not clear whether the measured polarization actually arises due to the cloud itself or it results from scattering in the tenuos interstellar medium. However, it is to be noted that the relation in Eq. 6.7 gives only an upperlimit and the interstellar polarization need not be as large as 2.7%. Besides, this estimate of the distance to the cloud, by assuming that it is associated with the cluster, has been found inconsistent with one made on the basis of star-count techniques (Lada et al 1994). From the lack of foreground stars seen towards the Northern Streamer, Lada et al suggest a star-count based distance of 400 pc to the

cloud, but declare these estimates to be highly uncertain. They also find that the visual extinction in the cloud varies over a large range within the extent of the cloud and this may explain the large scatter in the polarization level seen in our measurements.

If the observed polarization actually is originating due to scattering in the cloud, then the magnetic field as indicated by the polarization vectors, is mostly perpendicular to the cloud's long axis. Such a field, if it has sufficient strength, can support the cloud against collapsing normal to the field lines and might explain the elongated nature of the cloud. Since, a bimodal distribution of polarization position angles is not observed towards this cloud, filamentary cloud models with toroidal magnetic fields are probably not viable for this cloud.